TJ8.5 THE APPLICATION OF SATELLITE SEA-SURFACE SALINITY (SSS) OBSERVATIONS TO OPERATIONAL PASSIVE MICROWAVE RADIOMETRY

Eric Bayler*
NOAA/NESDIS Center for Satellite Applications and Research (STAR)

1. INTRODUCTION

Satellite sea-surface salinity (SSS) observations provide an avenue for reducing biases and uncertainty in those passive microwave observations having a significant surface emissivity term in their retrieval algorithm. While the Argo float program has helped address data-poor SSS *in situ* climatologies, these climatologies remain notably sparse in time and space, with a significant portion of the ocean having been rarely measured, if ever (Fig. 1). These *in situ* surface climatologies include observations down to depths of as much as 10 m, introducing uncertainty with respect to representativeness of the skin (~ 1 cm or less) salinity that is affecting the surface emissivity measured by satellite passive microwave instruments. Global satellite SSS coverage is now available every three days from the European Space Agency's (ESA) Soil Moisture – Ocean Salinity (SMOS) mission and weekly for NASA's Aquarius mission. Satellite SSS instruments use passive microwave retrieval algorithms to measure skin salinity; consequently, for passive microwave radiometry applications, satellite SSS will generally be more representative in space, time, and observed location within the water column than *in situ* climatologies. As technologically-new measurements, these data continue to be refined. This study examines the role of SSS in operational passive microwave radiometry and illustrates how SSS data choices affect results.

2. METHODOLOGY

The traceability of SSS to passive microwave brightness temperature (*Tb*) is examined first. Equation 1 relates polarized top-of-atmosphere brightness temperature ($Tb_p(\theta)$) to upwelling atmospheric brightness temperature ($Tb\uparrow(\theta)$), surface brightness temperature ($Tb_0(\theta)$) and polarized reflected sky brightness temperature ($Tb_p^s(\theta)$).

$$\mathrm{Tb_p}(\theta) = \mathrm{Tb}\uparrow(\theta) + \tau_{\mathrm{atm}}\left[\mathrm{Tb_0}(\theta) + \mathrm{Tb_p^s}(\theta)\right], \qquad (1)$$

where τ_{atm} is atmospheric transmissivity and θ is viewing angle. Focusing on the surface brightness term (Tb_0),

$$\mathrm{Tb_0}(\theta) = \mathrm{E_p}(\theta)\mathrm{T_{sfc}}, \qquad (2)$$

where E_p is polarized surface emissivity. Surface emissivity (ε_{sfc}) is, in turn, a function of SSS, comprising three components, the flat surface emissivity (ε_{flat}) plus modifications due to surface roughness (ε_{rough}) and foam (ε_{foam}).

$$\varepsilon_{sfc}(\upsilon,\theta,p,SST,SSS,U,\phi) = \varepsilon_{flat}(\upsilon,\theta,p,SST,SSS) + \varepsilon_{rough}(\epsilon_{flat},U,\phi) + \varepsilon_{foam}(U,\theta), \quad (3)$$

* *Corresponding author address:* Eric Bayler, NOAA/NESDIS/STAR, NOAA Science Center, Room 701, 5200 Auth Road, Camp Springs, MD 20746; e-mail: Eric.Bayler@noaa.gov.

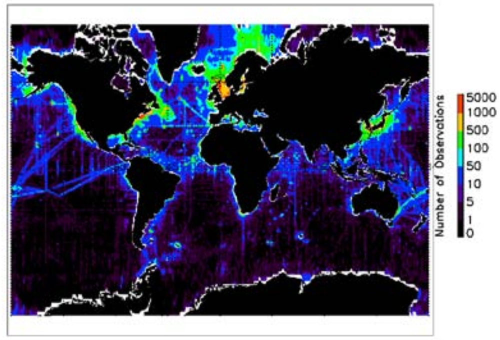

(a)

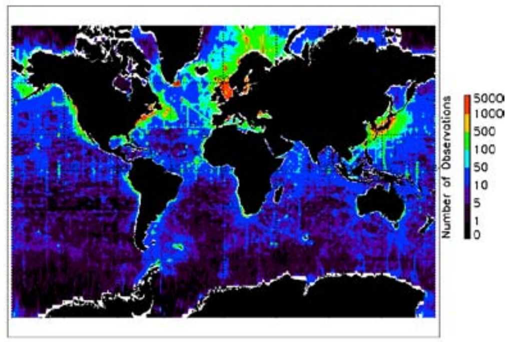

(b)

Fig. 1. NOAA's World Ocean Atlas: a) 1998 edition (Boyer *et al.,* 1998) depicts the accumulated number of SSS observations; b) the Argo float system, deployed over the next decade in conjunction with international partners, substantially increased SSS observations, as noted in the 2009 edition (Antonov *et al.*, 2010). Note the significant areas of the world's oceans still with no observations ever.

where ν is frequency, θ is viewing angle, *SSS* is sea-surface salinity, *SST* is sea-surface temperature, *p* is polarization, *U* is surface wind speed, and φ is wind direction. The sensitivity to SSS resides in the flat surface emissivity term (ε_{flat}). Polarized flat surface emissivity is computed by applying the Fresnel reflectivity equations to the ocean permittivity (dielectric constant) derived from empirical formulations. Typical empirical microwave permittivity models include dependencies on SSS, SST, and frequency. To enhance focus on SSS impacts, for this study the following base assumptions were made: flat sea, no wind, no foam, and an operationally-representative viewing angle (θ = 55°).

The empirical permittivity model used operationally by NOAA, a component of the Community Radiative Transfer Model (CRTM; Chen *et al.*, 2010) developed by the Joint Center for Satellite Data Assimilation (JCSDA), was used for computing Tb_0. The current operational CRTM configuration (v2.0.5) employs two permittivity models, one for frequencies less than 20 GHz (Guillou *et al.*, 1998) and the other for 20 GHz and higher (Lamkaouchi *et al.*, 1997). The higher-frequency is insensitive to SSS; therefore, the pending next-generation operational CRTM (v2.1) permittivity model was employed to examine SSS sensitivities for the higher frequencies above 20 GHz. Operational microwave frequencies of interest cluster around 6, 11, 19, 23, and 37 GHz. At higher frequencies, salinity variability has minimal impact on surface emissivity. Consequently, these representative frequencies were selected for evaluation. These frequencies are representative of the following satellite instruments: WindSat, Advanced Microwave Scanning Radiometer – EOS (AMSR-E), Tropical Rainfall Measuring Mission (TRMM) Microwave Imager (TMI), Special Sensor Microwave/Imager (SSMI/I), Special Sensor Microwave Imager / Sounder (SSMI/S), Advanced Microwave Sounding Unity (AMSU-A), and the Advanced Technology Microwave Sounder (ATMS).

NOAA's World Ocean Atlas (WOA; Antonov *et al*., 2010) climatological SSS and SST data were used for computing and comparing typically-used climatological Tb_0 values with Tb_0 values computed using newly-available quasi-near-real-time SSS values. The WOA climatological SST values (Locarnini *et al*., 2010) were used in both computations to limit differences to those produced by differences in SSS. Gridded SMOS SSS data developed by the SMOS Barcelona Expert Centre (SMOS-BEC) provided monthly mean SSS values for comparison with monthly WOA climatological values. This data (SMOS-BEC, 2008), comprised only ascending-node data retrieved using SMOS surface roughness model #1, was optimally-interpolated to a 100-km grid, with a temporal-averaging period of 30 days.

3. RESULTS AND ANALYSIS

This study aims to demonstrate that near-real-time SSS needs to be considered for passive microwave radiometry. Developmental satellite SSS data were used; therefore, interpreting specific differences needs to be tempered with acknowledgment that the results are not yet considered robust. It is also recognized that, when comparing the results for a single year with climatology, differences are to be expected due to how well that year's data represents climatology. For this study differences are defined as satellite SSS values minus climatological values.

Figure 2 illustrates higher-resolution features seen in satellite SMOS SSS data in contrast to the broad smooth features of the WOA SSS (Antonov *et al*., 2010). Broader patterns of differences (Figure 2.c) between quasi-near-real-time and climatological values potentially indicate spatial biases that could be removed from passive microwave retrievals. Likewise, addressing the annual cycle of these differences potentially could lead to reduced temporal biases in retrievals. More important than the spatial-temporal SSS difference features are the spatial-temporal difference of Tb_0 because it is the combination of temperature with the SSS-driven differences in surface emissivity that produce the surface brightness temperature biases of concern to passive microwave radiometry. Consequently, the differences discussed in this study are in terms of Tb_0 impacts. Vertically-polarized Tb_0 differences are an order of magnitude larger than horizontally-polarized Tb_0 differences, which are, for now, negligible, being of order 0.02° K. Spatial and temporal difference patterns for horizontally-polarized Tb_0 become notably more defined and a bit larger at the higher frequencies; however, the differences are still only of order 0.04° K. Vertically-polarized Tb_0 differences approach 0.5° K. Therefore, this study's discussion focuses on vertically-polarized Tb_0 differences.

Starting with the current operational CRTM (v2.0.5) permittivity model, monthly-mean Tb_0 differences are explored for frequencies 6 GHz, 11 GHz, and 19 GHz. Frequencies 23 GHz and 37 GHz experience no difference because, for frequencies 20 GHz and higher, the current operational CRTM (v2.0.5) is insensitive to salinity variations.

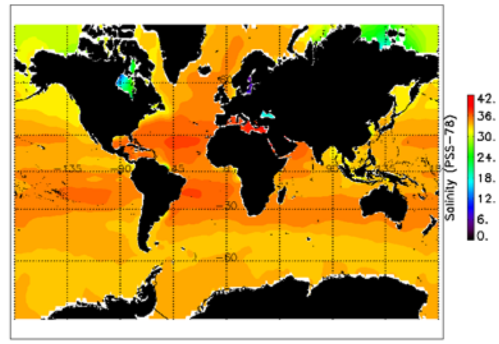

(a)

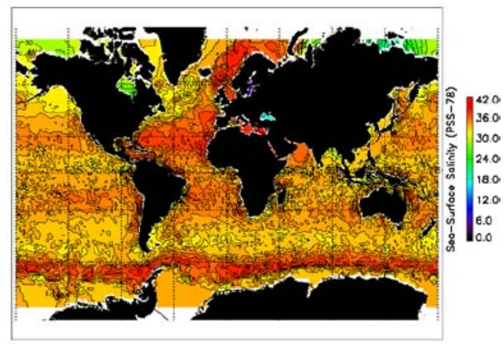

(b)

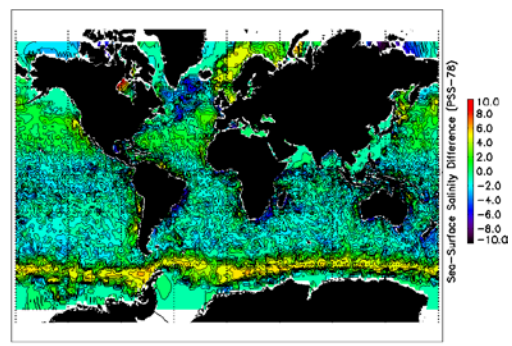

(c)

Fig. 2. Monthly-mean sea-surface salinity (SSS) for May: a) World Ocean Atlas (WOA) 1998 (Boyer *et al.*, 1998); b) SMOS-Barcelona Expert Centre data from 2011 (SMOS-BEC, 2008); SSS difference (SMOS-BEC minus WOA 1998).

At 6 GHz (Figure 3), representative months appear to indicate annual cycle variability in the region of the North Atlantic Drift, as well as along the western boundary of continents where upwelling is typical. The north coast of South America has a significant and enduring negative difference. The west coast of Norway has consistently negative differences that display a notable seasonal cycle. There also appears to be a bit of a signal in the vicinity of the Antarctic Circumpolar Current; although, this may change as more robust SSS values addressing wind-driven surface roughness issues are computed for the SMOS data. In a broad sense, anomalies are notably reduced in the summer, which correlates with the WOA's greater number of monthly observations due to the northern hemisphere field work season and the resulting greater representativeness of the WOA's SSS climatology. The tropics and

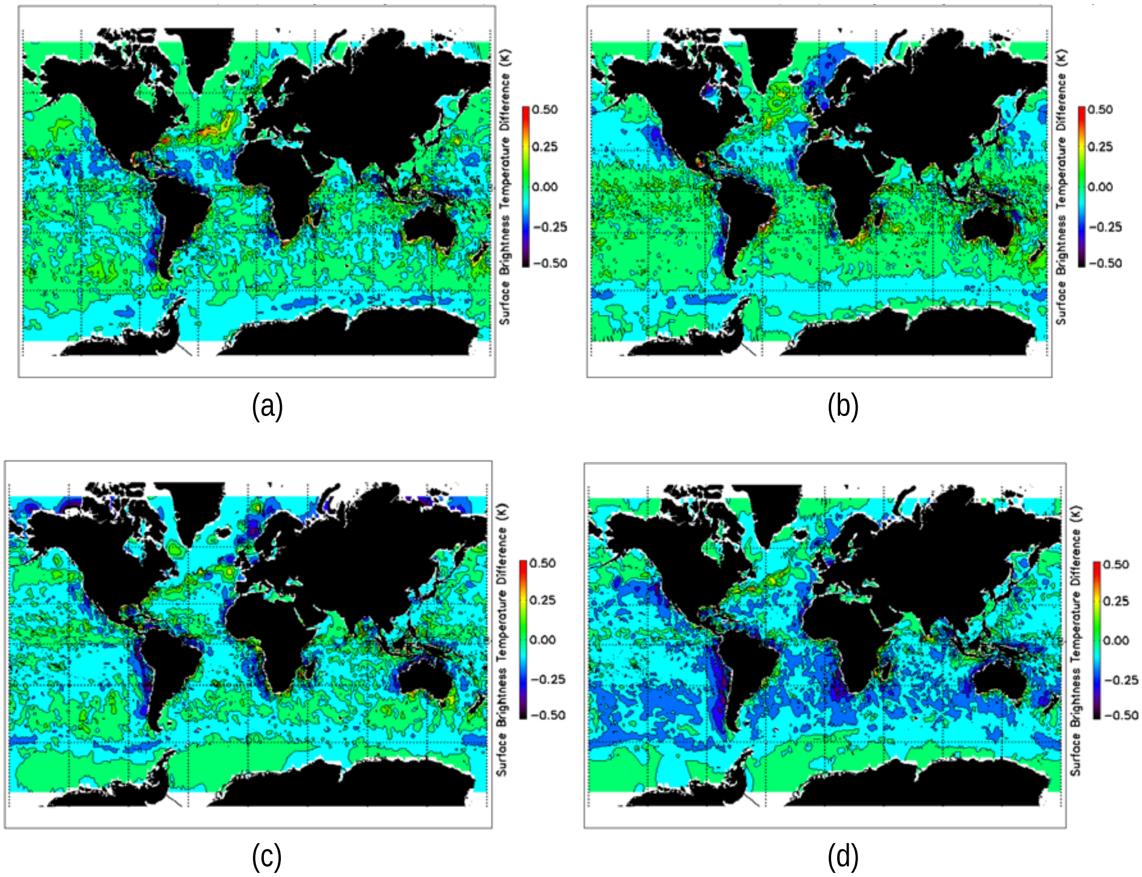

Fig. 3. Surface brightness temperature (Tb_0) differences (°K) at 6 GHz, derived, using the Community Radiative Transfer Model v2.0.5 (Chen *et al.*, 2010) from SMOS-BEC sea-surface salinity (SMOS-BEC, 2008) minus Tb_0 derived from World Ocean Atlas 1998 sea-surface salinity (Boyer *et al.*, 1998): a) February, b) May, c) August, and d) November.

subtropics tend toward weakly positive differences February through September through December values display broad negative differences, with October having the most intense differences.

As expected, the 11 GHz Tb_0 difference patterns (Figure 4) are quite similar to those at 6 GHz, with the differences being at 11 GHz being a somewhat muted. Areas where differences stand out are include the Gulf Stream and North Atlantic Drift appear as the most notable positive difference; however, there is no corresponding signature for the Kuroshio Current in the Pacific Ocean. Significant negative differences include eastern boundary currents or collocated upwelling regions, as well as along the Norwegian Current. The Antarctic Circumpolar Current region has minimal differences. At 19 GHz, the general patterns and notable features remain (Figure 5), but the Tb_0 differences are noticeably more muted, with broad swaths of ocean basins tending toward minimal difference, consistent with diminishing sensitivity of surface emissivity to salinity as frequency increases.

Next, repeating the same analysis using the pending new operational CRTM permittivity model (v2.1) highlights differences resulting from how the new and old models incorporate the salinity dependency in the empirical formulation of permittivity. Figure 6 depicts, as a function of SSS and frequency, the difference between the Tb_0 produced by the pending CRTM v2.1 and the existing CRTM v2.0.5. In addition to differences due to empirical formulations, CRTM v2.1 provides a continuous across frequencies, eliminating the discontinuity existing in CRTM 2.0.5. At 6 GHz (Figure 7), the August, with the greatest positive differences appearing in June. most notable difference from Figure 3 is the strong negative difference along the Antarctic Circumpolar Current. In general the other patterns are largely similar; although, the v2.1 model exhibits wider-spread stronger differences, of order 0.5° K. Few differences are noted between the results at 11 GHz for the new v2.1 model (Figure 8) and the existing v2.0.5 model (Figure 4). At 19 GHz (Figure 9), the v2.1 model differences are notable more muted than the v2.0.5 differences, yet there are still distinct features that would create spatial biases as large as 0.25° K, demonstrating the significance of SSS observations to passive microwave retrievals at this frequency. An interesting observation is the trend from negative differences to positive differences in Antarctic Circumpolar Current region. The negative difference along the north coast of South America remains significant.

Using the v2.1 permittivity model to explore SSS sensitivity for the operational frequencies above 20 GHz, reveals the continued trend of increasingly muted differences in Tb_0. Figure 10, the Tb_0 differences at 23 GHz, depicts the continuing trend of increasingly positive differences along the Antarctic Circumpolar Current. Most other explicit signatures have vanished, except the negative differences along the west and north coasts of South America and the west coast of Africa. The Gulf Stream – North Atlantic Drift has only a minor signature. At 37 GHz (Figure 11), the only remaining significant features are the increasingly positive difference along the Antarctic Circumpolar Current that reaches about 0.25° K in places

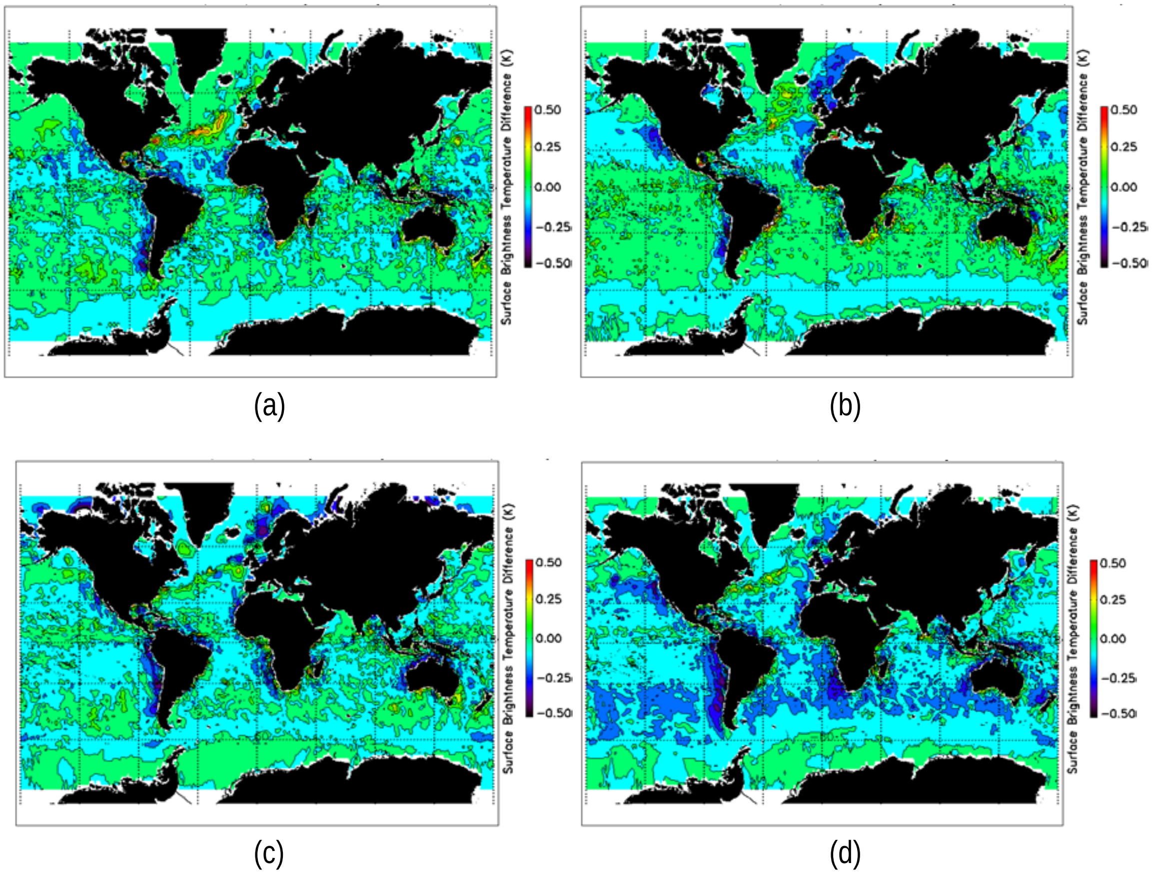

Fig. 4. Surface brightness temperature (Tb_0) differences (°K) at 11 GHz, derived, using the Community Radiative Transfer Model v2.0.5 (Chen *et al.*, 2010) from SMOS-BEC sea-surface salinity (SMOS-BEC, 2008) minus Tb_0 derived from World Ocean Atlas 1998 sea-surface salinity (Boyer *et al.*, 1998): a) February, b) May, c) August, and d) November.

and the much diminished feature along the north coast of South America.

4. CONCLUSIONS

Clearly, SSS is a factor in passive microwave retrievals that have a significant ocean surface term. It is only just now that observations are becoming available to address this sensitivity and the spatial and temporal biases introduced by the current use of highly-sparse climatologies in passive microwave retrievals. Using the current SSS climatologies introduces uncertainty due to non-representativeness, even at the resolution of the climatologies. The new ability to observe SSS globally in quasi-near-real time provides the opportunity to improve passive microwave retrievals and dependent applications by employing those SSS observations directly in retrievals. Looking ahead, in addition to integrating SSS observations, passive microwave radiometry algorithms, particularly those employing frequencies across the 20 GHz discontinuity in the existing CRTM v2.0.5 model, need to examine the impact of the change to the new permittivity model in the CRTM v2.1 model. Retrievals employing frequencies above 20 GHz and relying on the CRTM model for computing ocean surface emissivity are now insensitive to salinity variability; however, when implementing CRTM v2.1, there will be a jump in emissivity values produced from the same input values, as well as the addition of a salinity dependency.

5. ACKNOWLEDGMENTS

Data provided by the European Space Agency and the SMOS Barcelona Expert Centre. The views, opinions, and findings contained in this report are those of the author and do not constitute a statement of policy, decision, or position on behalf of National Oceanic and Atmospheric Administration (NOAA) or the U.S. Government.

6. REFERENCES

Antonov, J. I., D. Seidov, T. P. Boyer, R. A. Locarnini, A. V. Mishonov, H. E. Garcia, O. K. Baranova, M. M. Zweng, and D. R. Johnson, World Ocean Atlas 2009, Volume 2: Salinity. S. Levitus, Ed. NOAA Atlas NESDIS 69, U.S. Government Printing Office, Washington, D.C., 2010.

Boyer, T. P., Levitus, S., J. Antonov, M. Conkright, T. O' Brien, C. Stephens. World Ocean Atlas 1998. Vol. 4, Salinity of the Atlantic Ocean. Silver Spring, MD : U.S. Dept. of Commerce, National Oceanic and Atmospheric Administration, National Environmental Satellite, Data and Information Service, National Oceanographic Data Center, Ocean Climate Laboratory, 1998. (*NOAA atlas NESDIS* ; 30.) G1046.C1 N3 no.30.

Boyer, T.P., Levitus, S., J. Antonov, M. Conkright, T. O' Brien, C. Stephens. World Ocean Atlas 1998. Vol. 5, Salinity of the Pacific Ocean. Silver Spring, MD : U.S. Dept. of Commerce, National Oceanic and Atmospheric Administration, National Environmental Satellite, Data and Information Service, National Oceanographic Data Center, Ocean Climate Laboratory, 1998. (*NOAA atlas NESDIS* ; 31.) G1046.C1 N3 no.31

Boyer, T. P., Levitus, S., J. Antonov, M. Conkright, T. O' Brien, C. Stephens, B. Trotsenko. World Ocean Atlas 1998. Vol. 6, Salinity of the Indian Ocean. Silver Spring, MD : U.S. Dept. of Commerce, National Oceanic and Atmospheric Administration, National Environmental Satellite, Data and Information Service, National Oceanographic Data Center, Ocean Climate Laboratory, 1998. (*NOAA atlas NESDIS* ; 32.) G1046.C1 N3 no.32.

Chen, Y., Y. Han, P. Van Delst, and F. Weng, "On water vapor Jacobian in fast radiative transfer model," *J. Geophys. Res.*, 115, D12303, doi:10.1029/2009JD013379, 2010.

Guillou, C., W. Ellison, L. Eymard, K. Lamkaouchi, C. Prigent, G. Delbos, G. Balana, and S. A. Boukabara, "Impact of new permittivity measurements on sea surface emissivity modeling in microwaves," *Radio Science,* vol. 33, no. 3, pp. 649-667, 1988.

Lamkaouchi K., A. Balana andW.J. Ellison, "New permittivity data for sea water (30-100 GHz)", Extension of ESA report 11197/94/NL/CN, 1997.

Liu, Q., F. Weng, and S. English, "An improved fast microwave water emissivity model," *IEEE Trans. Geosci. Remote Sensing*, 2010, DOI: 101109/TGRS.20102064779.

Locarnini, R. A., A. V. Mishonov, J. I. Antonov, T. P. Boyer, H. E. Garcia, O. K. Baranova, M. M. Zweng, and D. R. Johnson, World Ocean Atlas 2009, Volume 1: Temperature. S. Levitus, Ed. NOAA Atlas NESDIS 68, U.S. Government Printing Office, Washington, D.C., 2010.

SMOS Barcelona Expert Centre, "SMOS CP34 OS L3 Algorithm Theoretical Baseline Document", CP34-ATBD-OS-0001 Issue 2 Rev 3, 2008.

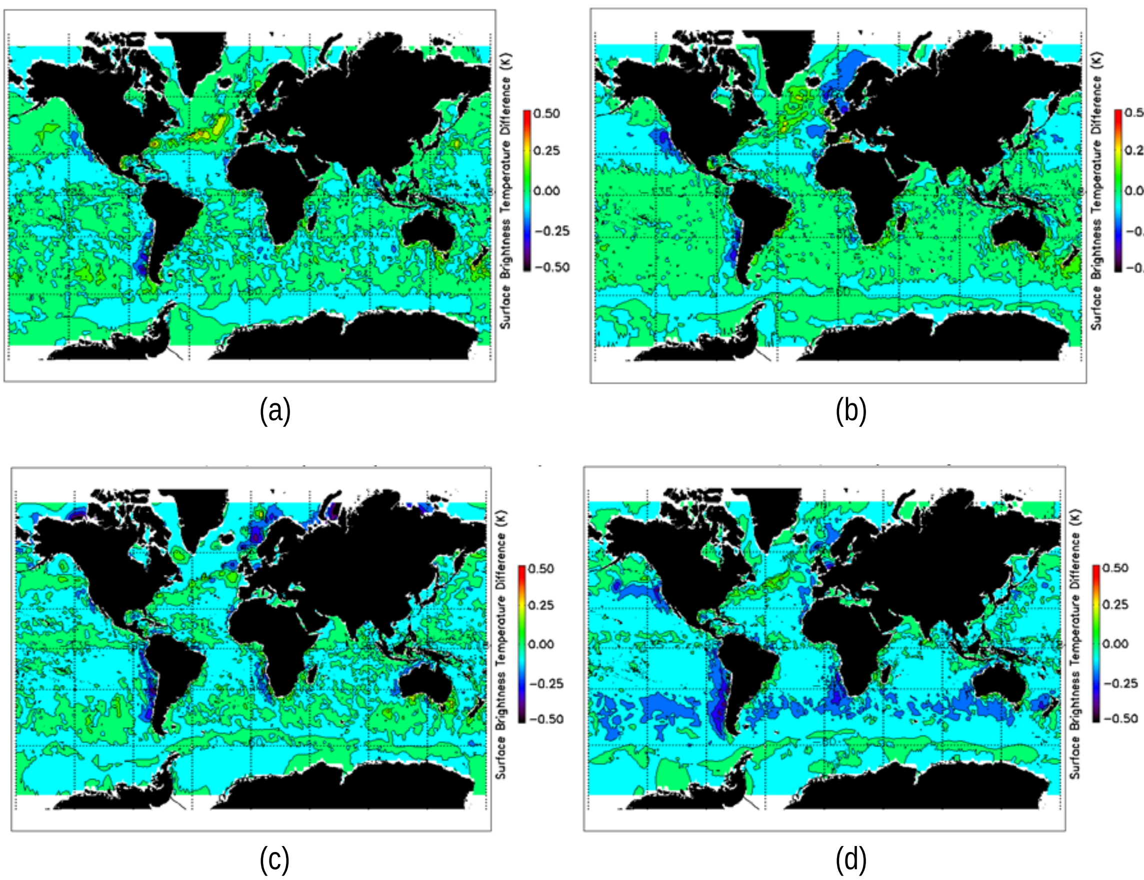

Fig. 5. Surface brightness temperature (Tb_0) differences (°K) at 19 GHz, derived, using the Community Radiative Transfer Model v2.0.5 (Chen *et al.*, 2010) from SMOS-BEC sea-surface salinity (SMOS-BEC, 2008) minus Tb_0 derived from World Ocean Atlas 1998 sea-surface salinity (Boyer *et al.*, 1998): a) February, b) May, c) August, and d) November.

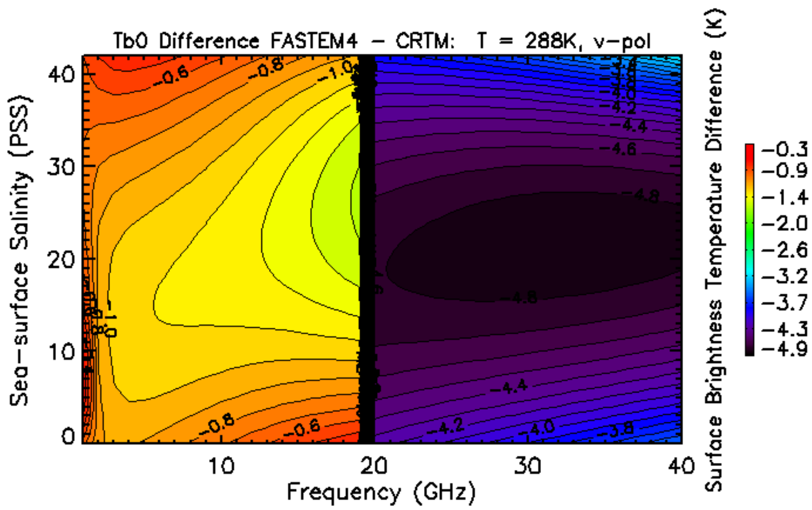

Fig. 6. Surface brightness temperature (Tb_0) differences (°K), as a function of frequency and sea-surface salinity at 288°K,between Community Radiative Transfer Model (CRTM; Chen *et al*., 2010) v2.1 and v2.0.5 highlight the changes that will occur across the 20 GHz discontinuity in CRTM 2.0.5 when implementing CRTM v2.1.. The new emissivity model in CRTM v2.1 is also referred to as FASTEM4.

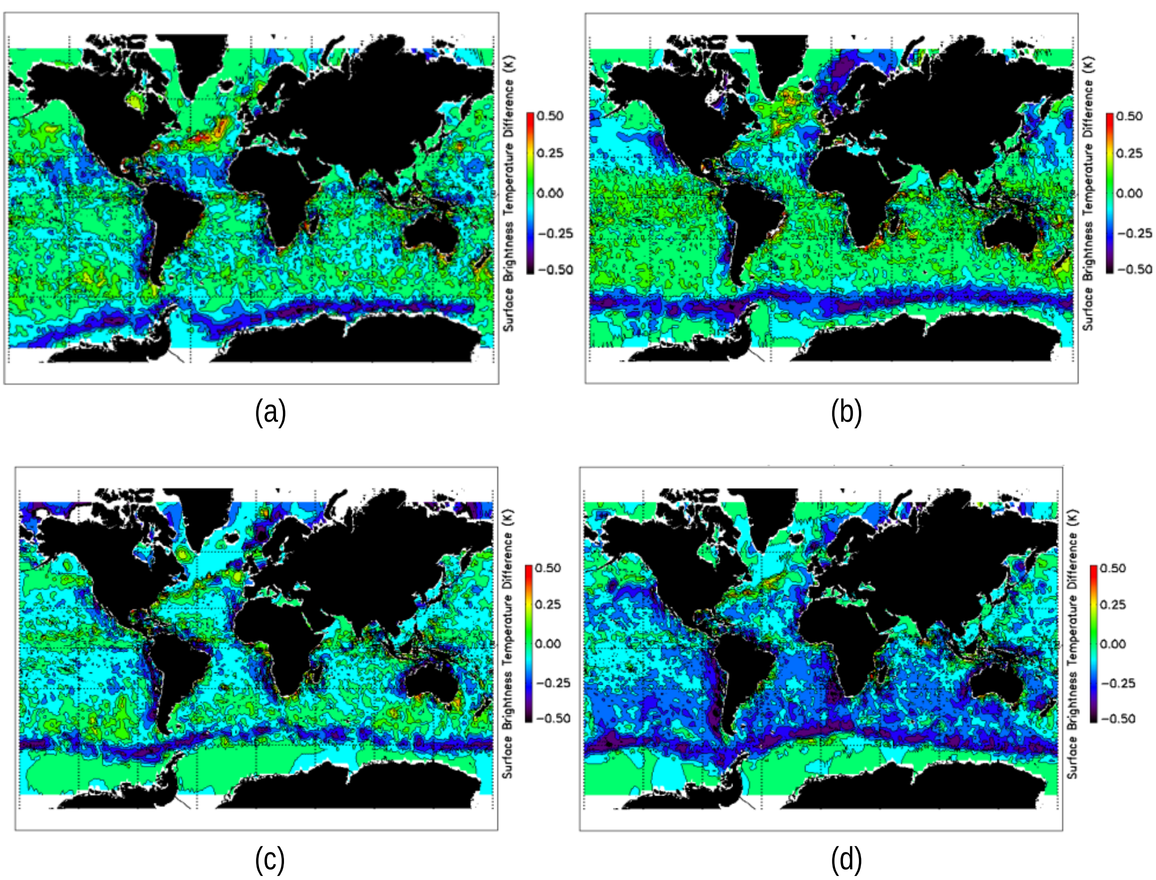

Fig. 7. Surface brightness temperature (Tb_0) differences (°K) at 6 GHz, derived, using the Community Radiative Transfer Model v2.1 (Chen *et al.*, 2010) from SMOS-BEC sea-surface salinity (SMOS-BEC, 2008) minus Tb_0 derived from World Ocean Atlas 1998 sea-surface salinity (Boyer *et al.*, 1998): a) February, b) May, c) August, and d) November.

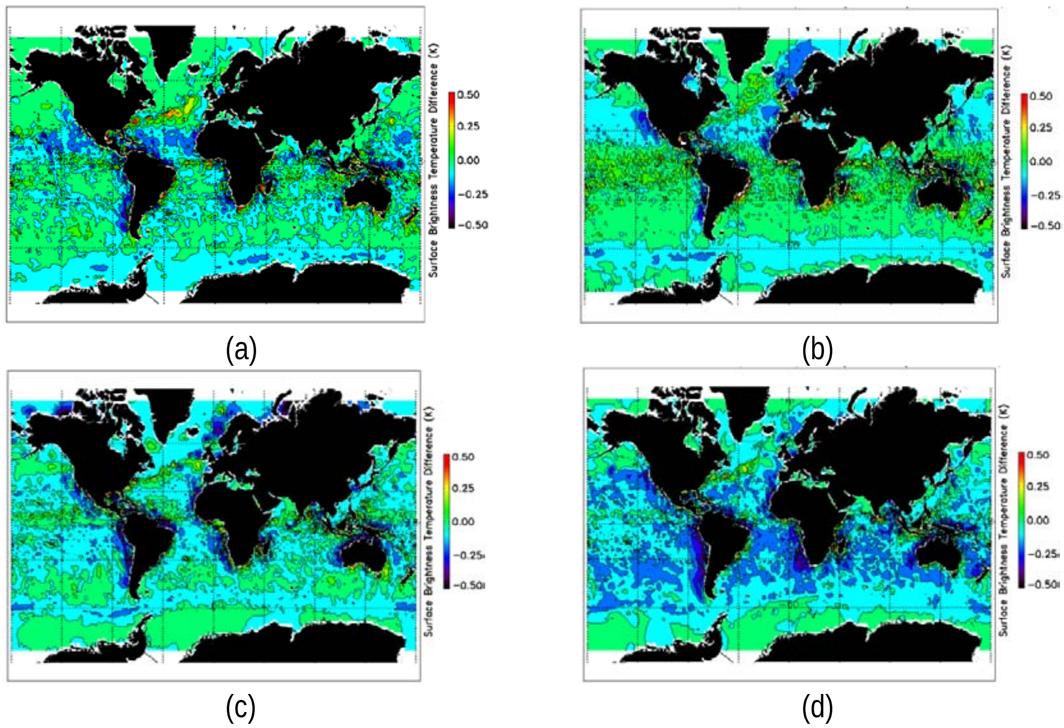

Fig. 8. Surface brightness temperature (Tb_0) differences (°K) at 11 GHz, derived, using the Community Radiative Transfer Model v2.1 (Chen *et al.*, 2010) from SMOS-BEC sea-surface salinity (SMOS-BEC, 2008) minus Tb_0 derived from World Ocean Atlas 1998 sea-surface salinity (Boyer *et al.*, 1998): a) February, b) May, c) August, and d) November.

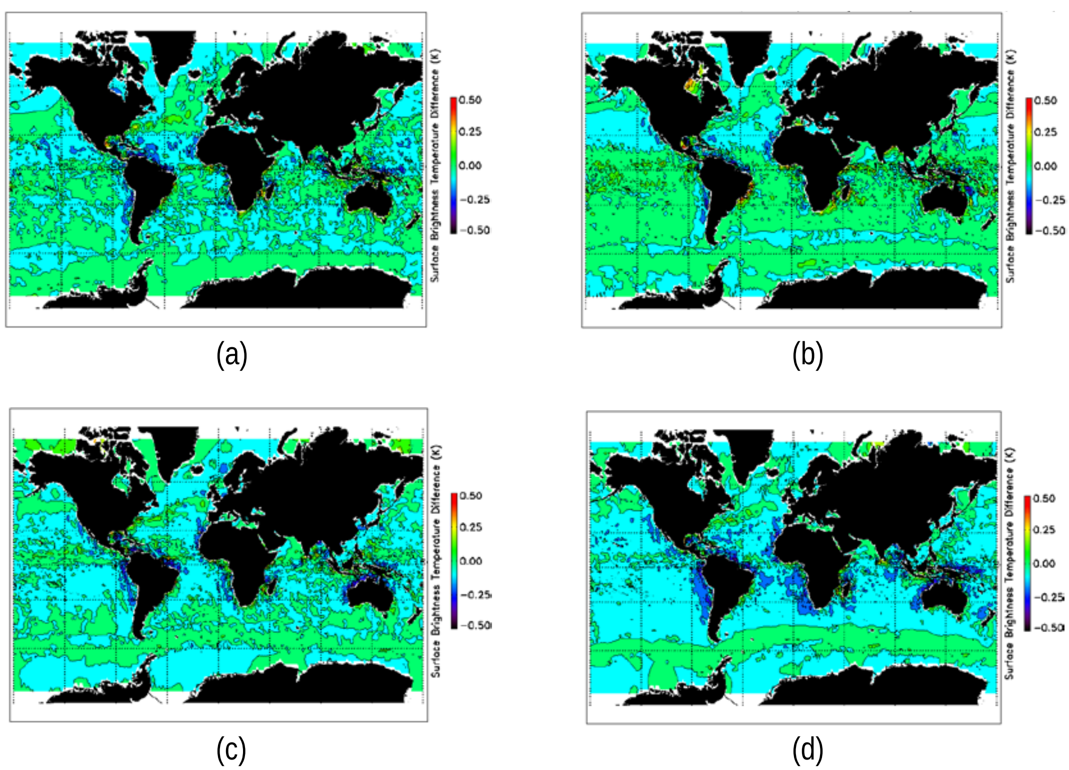

Fig. 9. Surface brightness temperature (Tb_0) differences (°K) at 19 GHz, derived, using the Community Radiative Transfer Model v2.1 (Chen *et al.*, 2010) from SMOS-BEC sea-surface salinity (SMOS-BEC, 2008) minus Tb_0 derived from World Ocean Atlas 1998 sea-surface salinity (Boyer *et al.*, 1998): a) February, b) May, c) August, and d) November.

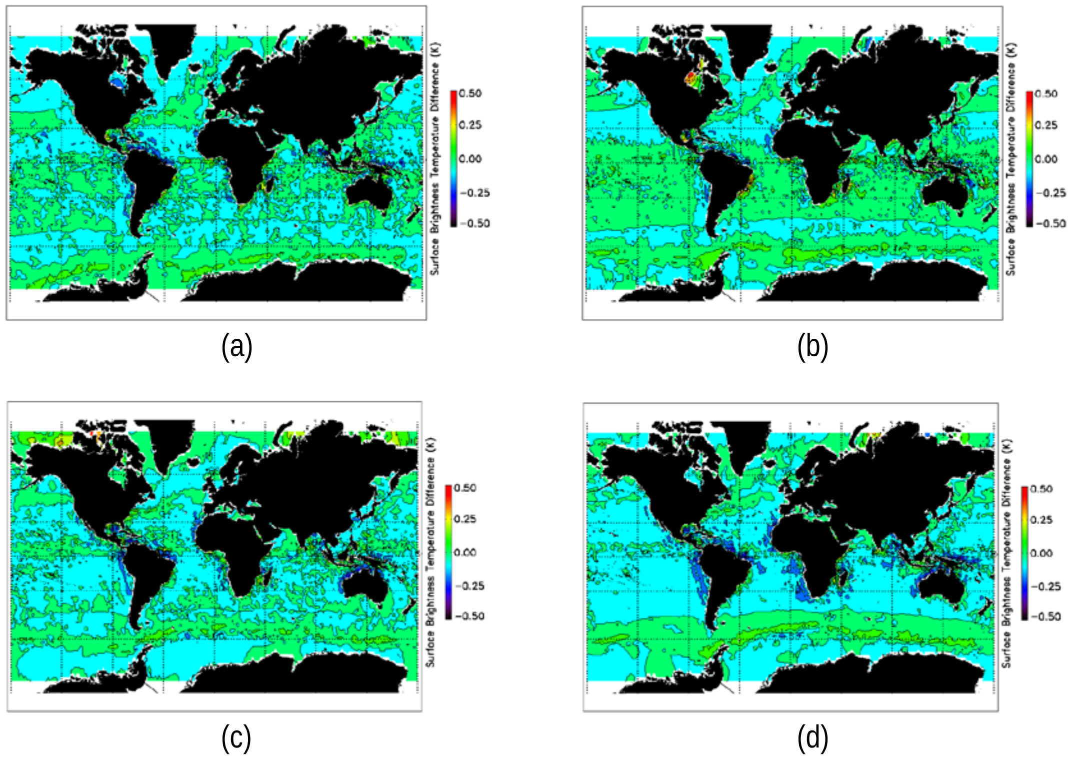

Fig. 10. Surface brightness temperature (Tb_0) differences (°K) at 23 GHz, derived, using the Community Radiative Transfer Model v2.1 (Chen *et al.*, 2010) from SMOS-BEC sea-surface salinity (SMOS-BEC, 2008) minus Tb_0 derived from World Ocean Atlas 1998 sea-surface salinity (Boyer *et al.*, 1998): a) February, b) May, c) August, and d) November.

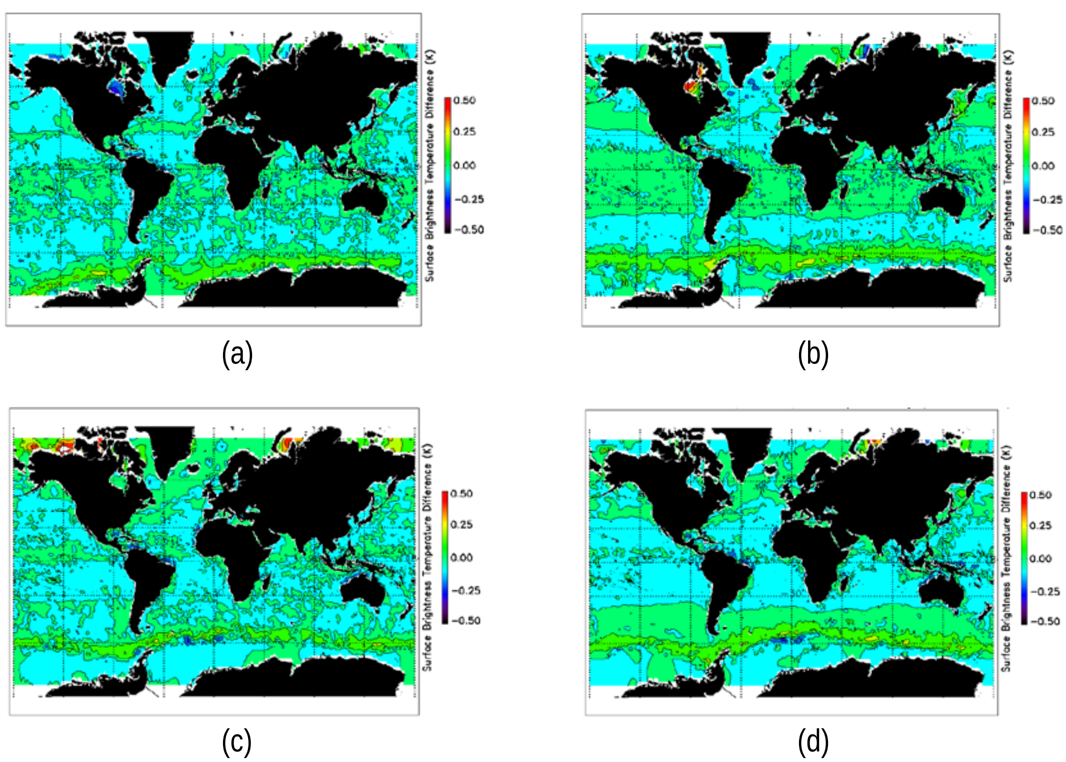

Fig. 11. Surface brightness temperature (Tb_0) differences (°K) at 37 GHz, derived, using the Community Radiative Transfer Model v2.1 (Chen *et al.*, 2010) from SMOS-BEC sea-surface salinity (SMOS-BEC, 2008) minus Tb_0 derived from World Ocean Atlas 1998 sea-surface salinity (Boyer *et al.*, 1998): a) February, b) May, c) August, and d) November.